ARTICLE

Magnetic and Nonmagnetic Nanoparticles from a Group of Uniform Materials Based on Organic Salts

Aaron Tesfai,[†] Bilal El-Zahab,[†] Algernon T. Kelley,[†] Min Li,[†] Jayne C. Garno,[†] Gary A. Baker,[‡] and Isiah M. Warner[†,*]

[†]Department of Chemistry, Louisiana State University, Baton Rouge, Louisiana 70803, and [‡]Chemical Sciences Division, Oak Ridge National Laboratory, Oak Ridge, Tennessee 37831

ABSTRACT The size and uniformity of magnetic nanoparticles developed from a *g*roup of *u*niform *m*aterials *b*ased on *o*rganic *s*alts (GUMBOS) were controlled using an *in situ* ion exchange, water-in-oil (w/o) microemulsion preparation. Most of these nanoGUMBOS are in fact ionic liquids (*i.e.*, melting points less than 100 °C), while others have melting points above the conventional 100 °C demarcation. Simple variations in the reagent concentrations following a w/o approach allowed us to smoothly and predictably vary nanoparticle dimensions across a significant size regime with excellent uniformity. Average sizes of GUMBOS particles ranging from 14 to 198 nm were achieved by manipulation of the reagent concentration, for example. Controllable formation of this new breed of nanoparticles is important for numerous potential applications and will open up interesting new opportunities in drug delivery, magnetic resonance imaging, and protein separations, among other areas.

KEYWORDS: nanosynthesis · emulsion · molten salt · ionic liquids · GUMBOS · reverse micelles · magnetic nanoparticles

Ionic liquids (ILs) are defined as molten salts with melting points at or below 100 °C.[1,2] Unlike conventional salts, such as sodium chloride, ILs are typically formed from bulky asymmetric organic cations paired to partially fluorinated anions which serve to make packing highly inefficient, resulting in melting points near ambient.[3] In this paper, we investigate a novel class of material we have given the acronym GUMBOS, defined as a *g*roup of *u*niform *m*aterials *b*ased on *o*rganic *s*alts. While our study encompasses salts which are formally ILs by the typical definition, GUMBOS are also inclusive of related organic salts with melting points above 100 °C. Thus, GUMBOS are intriguingly useful ionic materials which retain the designer versatility of ILs, in that a manipulation of either the anion or the cation structure/functionality may yield significant changes in physicochemical properties, allowing them to be devised for a host of applications.[4,5] We note that the term "room temperature ionic liquid" (RTIL) has typically been reserved for salts that are liquid at room temperature (*i.e.*, 25 °C). RTILs have been employed for applications such as chromatography,[6] extractions,[7] catalysis,[8] and nanosynthesis.[9,10] Recently, RTILs have also been used as supports for the synthesis of nanowires,[11] as dispersants to regulate the shape of nanorods,[12] and as a dispersed phase in IL/oil emulsions to regulate the growth of hierarchical macroporous metal oxides.[13]

Aside from the use of ILs as solvents and in other liquid-state applications, very little focus has been given to ILs and their tunability in the solid state. In 2007, Rutten *et al.* employed frozen ILs (ILs with melting points exceeding ambient, thus remaining ionic solids near room temperature) as substrates for rewritable imaging.[14] More recently, our group reported the first nano- and microparticles developed from the frozen IL 1-butyl-2,3-dimethylimidazolium hexafluorophosphate ([bm_2Im][PF_6]) using a novel melt−emulsion−quench approach.[15] Herein we report the first examples of nanoGUMBOS with functionality capable of mimicking the properties of usual nanoparticles with the task-specific properties of ILs.

In recent years, magnetic nanoparticles have garnered considerable interest in various disciplines such as drug delivery,[16] separations,[17] magnetic resonance imaging,[18] and cancer hyperthermia treatment.[19] Iron oxide nanoparticles with diameters typically around 10−20 nm exhibit superparamagnetism and can be magnetized in the presence of an external magnetic field and readily redispersed in the absence of a field with negligible particle aggregation.[20] For many of these applications, modifying the surface of the nanosized magnetic particles can be a considerably difficult and tedious task. Surface modifica-

*Address correspondence to iwarner@lsu.edu.

Received for review July 10, 2009 and accepted September 11, 2009.

Published online September 25, 2009.
10.1021/nn900781g CCC: $40.75

tion is typically achieved by physically adsorbing or chemically attaching molecules to the nanoparticle surface. For example, in an article by Hong *et al.*,[21] to synthesize fluorescent magnetic nanoparticles, the process first started by separately preparing iron oxide nanoparticles and quantum dots. Next, a complex linking process to combine the dual functionality of the fluorescent and magnetic particles was employed using polymeric materials. Due to the inherent nature of the linking process and lack of control over cross-linking-caused aggregation, typically the functionalization task is neither simple nor does it produce uniformly functionalized particles. In addition, commonly used metal oxide nanoparticles (*e.g.*, Fe_2O_3, NiO, $CoFe_2O_3$) are relatively toxic and require benign coatings (*e.g.*, polyethylene glycol) for biological applications which further restricts their use *in vivo*.[22] Therefore, routes to biocompatible magnetic nanoparticles with tunable properties that can be easily tailored to a specific application remain of paramount importance. GUMBOS are immediately pertinent in that aspect since they can be designed to be nontoxic and might even play a medicinal or nutritive role by synthesizing GUMBOS from environmentally responsible "green" materials including various vitamins, amino acids,[23] artificial sweeteners,[24] nutraceuticals, drugs,[25] and phytochemicals.

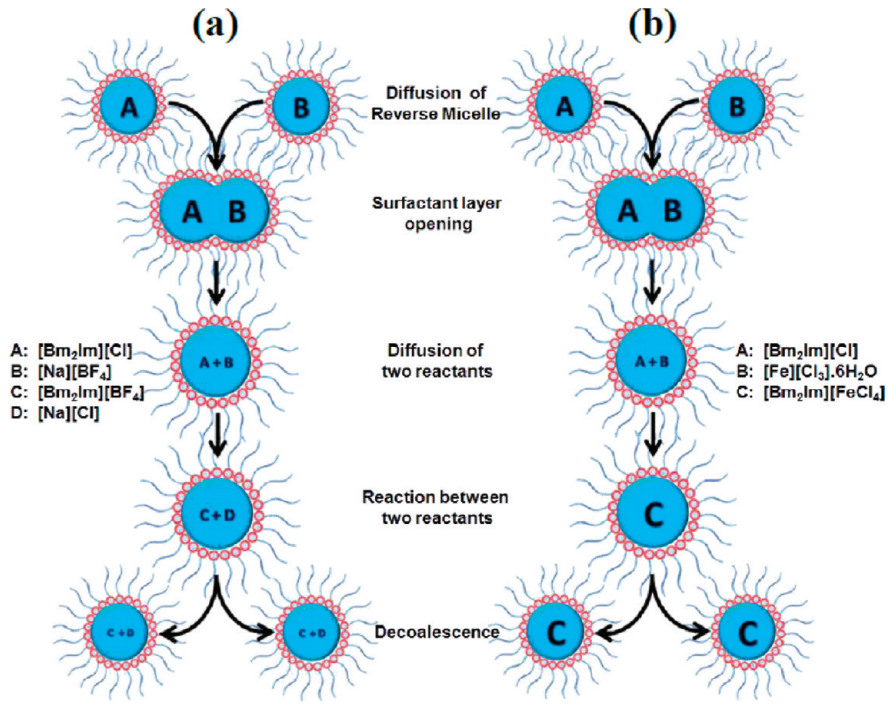

Scheme 1. Basic processes for nanoparticle formation within AOT reverse micelles. Individual reverse micelles are shown without free surfactants:[33] (a) $[Bm_2Im][BF_4]$ nanoGUMBOS; (b) $[Bm_2Im][FeCl_4]$ magnetic GUMBOS particles.

ILs with anions containing transition metal complexes have recently sparked considerable interest.[26−28] Although these ILs were among the earliest developed, their magnetic behavior was largely overlooked.[26] The first report of a magnetic IL, 1-butyl-3-methylimidazolium tetrachloroferrate ([Bmim][$FeCl_4$]), and its response to a magnetic field appeared in 2004.[27] To our knowledge, however, the synthesis of a nanoscale material composed solely from magnetic ILs/GUMBOS has yet to be reported. We hypothesize that magnetic nanoGUMBOS will hold significant advantages as compared to other common magnetic nanoparticles because they should also exhibit the tunability and inherent functionality of ILs. In addition, both the anion and the cation may carry unique functional properties, allowing dual or polyfunctional nanoGUMBOS to be prepared. This tunability will ultimately provide superior control over relevant properties of the nanoparticles, such as solubility[29] and melting point.[30] When paired with particle size control, this provides an ideal platform for targeted drug delivery, as well as for sensory and imaging applications.

Challenges encountered in the synthesis of monodispersed nanoparticles have led to extensive research into size control by use of various organized media.[31,32] For example, aerosol-OT (AOT, sodium bis(2-ethylhexyl)sulfosuccinate), a well-studied surfactant, is known to form stable and spherical reverse micelles in nonpolar solvents such as *n*-heptane.[33] Use of these reverse micellar templates for nanoparticle formation often leads to relatively monodispersed nanoparticles with controlled sizes due to the ability of this reverse micelle system to stabilize relatively large water pools of defined sizes.[34,35]

In this paper, we report the initial synthesis and behavior of particles composed of GUMBOS containing both the BF_4^- and the $FeCl_4^-$ anion and demonstrate the tunability of their physicochemical properties evident *via* changes in the cationic component of the GUMBOS. In this current work, we employ AOT reverse micelles as templates to exert size control over the resultant liquid and solid GUMBOS particles. Parameters such as surfactant concentration, water-to-surfactant molar ratio, temperature, and solvent composition were optimized for size-targeted GUMBOS particles synthesis. The synthesized GUMBOS particles were characterized using transmission electron microscopy (TEM), UV−visible absorption spectroscopy (UV−vis), atomic force microscopy (AFM), and measurements using a superconducting quantum interference device (SQUID).

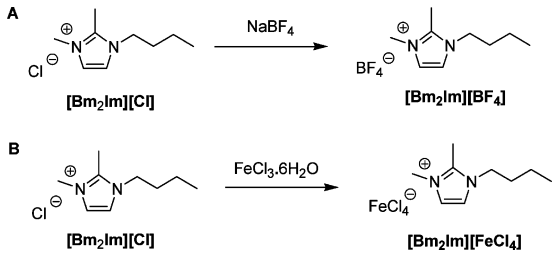

Scheme 2. Exchange reaction at (A) the micellar core and (B) magnetic GUMBOS synthesis at the micellar core.

RESULTS AND DISCUSSION

Particle Size Control. NanoGUMBOS composed of $[Bm_2Im][BF_4]$ and $[Bm_2Im][FeCl_4]$ GUMBOS particles were prepared following an AOT templating reverse micellar method.[28] The exchanging salts which yielded the GUMBOS were solubilized separately in the water pools of two water-in-oil microemulsions. After combining the two parent solutions, the formation of particles followed the steps outlined in Scheme 1 in the following order: (1) diffusional approach of reverse micelles; (2) surfactant layer opening and micellar coalescence; (3) diffusion of solubilized molecules within the merged reverse micelles; (4) metathesis or reaction between solubilized species with concomitant formation of product(s); and (5) decoalescence of reverse micelles carrying a GUMBOS particles payload (Scheme 2).[33] It is notable that the pockets of water formed in the core of the reverse micelles act as nanoreactors for the synthesis of these nanoparticles, while the use of self-assembled surfactants limits the particle growth to produce small and stable particles by providing a protective layer to preserve the microdroplets.[33]

Nonmagnetic NanoGUMBOS of $[Bm_2Im][BF_4]$. Nonmagnetic $[Bm_2Im][BF_4]$ nanoGUMBOS were prepared using the *in situ* ion exchange emulsion preparation outlined above, as summarized in Scheme 1a. Particle size control was easily achieved by careful variation in the surfactant and reactant concentrations, choice of nonpolar solvent, temperature, mixing regime, and the relative water volume. In terms of the latter, the level of water within the water pool is defined as the molar ratio of water to surfactant, ω_0. It was observed that controlled changes in the concentrations of reactants directly regulated the average size of the harvested nanoGUMBOS. Using reactant concentrations in the 0.2−0.6 M range at a fixed A/B molar ratio of 1:1 (Scheme 1), average nanoparticle diameters of 14.7 ± 2.2 to 68.0 ± 17.0 nm were obtained for 0.1 M AOT in *n*-heptane at a water loading ($\omega_0 = [H_2O]/[AOT]$) of 13.34. Panels a−d of Figure 1 present representative TEM images of $[Bm_2Im][BF_4]$ nanoGUMBOS with average sizes of 14.7, 20.8, 34.3, and 68.0 nm using initial concentrations of 0.2, 0.4, 0.5, and 0.6 M reagent, respectively. NanoGUMBOS shown in Figure 1 appear nonaggregated and uniformly dispersed on the carbon film of the TEM grid. The entire surface is covered with relatively uniformly sized particles with standard deviations of 2.2 nm for Figure 1A and 1.8 nm for Figure 1B. In contrast, the particles shown in Figures 1C,D are scattered more sparsely on the surface, although the relative standard deviation (RSD) in the particle size remains quite good. In fact, across the entire range of nanoGUMBOS synthesized, the RSD in particle size is near 15%. A higher polydispersity might be expected for the larger nanoGUMBOS. The underlying reason for this observation is that higher concentrations of reactants afford higher ion exchange and reactant diffusional collision rates, shifting the equilibrium-driven coalescence and decoalescence of the reverse micelles during particle formation. Table 1 is a presentation of data on the increase in diameter of $[Bm_2Im][BF_4]$ nanoGUMBOS with increasing reagent

TABLE 1. Effect of Reagent Concentration on Particle Size[a]

reagent concentration (M)	particle size (nm)	standard deviation (nm)
0.2	14.7	2.2
0.4	20.8	1.8
0.5	34.3	4.8
0.6	68.0	17

[a] $\omega_0 = 13.34$, molar ratio = 1:1, AOT concentration = 0.1 M.

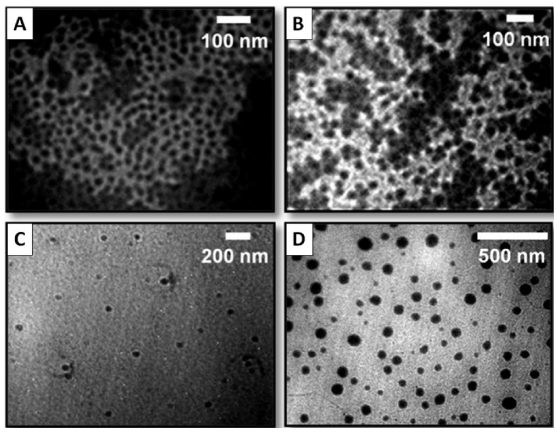

Figure 1. TEM micrographs of $[Bm_2Im][BF_4]$ nanoGUMBOS synthesized according to the approach shown in Scheme 1 and imaged by TEM at the indicated magnifications with average nanoparticle diameters of (A) 14.7 ± 2.2 nm, (B) 20.8 ± 1.8 nm, (C) 34.3 ± 4.8 nm, and (D) 68.0 ± 17.0 nm. Images were taken using an LVEM5 electron microscope with an accelerating voltage of 5 kV without staining.

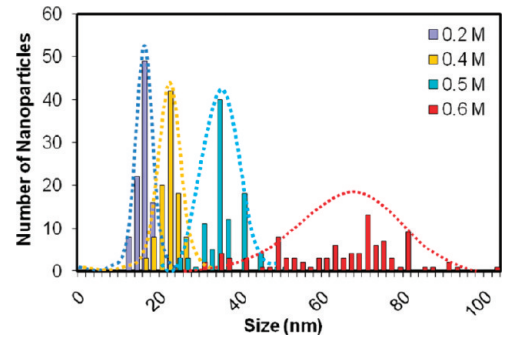

Figure 2. Size distributions of nanoGUMBOS synthesized *via* Scheme 1 in water-containing AOT reverse micelles at various reagent concentrations: [AOT] = 0.1 M; molar reagent concentrations = 0.2, 0.4, 0.5, and 0.6 M.

concentrations. Histogram plots summarizing the $[Bm_2Im][BF_4]$ nanoGUMBOS size distributions resulting from analysis of TEM results are furnished in Figure 2. This result clearly illustrates that the nanoGUMBOS particle size can be smoothly modulated simply by control over the reagent concentrations, a boon for simple, uniform nanoparticle production.

Simultaneously acquired topography and phase AFM images of nanoGUMBOS dried on mica are displayed in Figure 3 at two different magnifications. These particles are observed to possess highly spherical shapes ranging from 20 to 120 nm in diameter. Aggregation with neighboring particles is minimal, despite the fact that roughly 10% of the imaged surface is covered with particulate. The nanoscale variations in sizes are well apparent in the wide area frames ($60 \times 60\ \mu m^2$) of Figure 3A,B. There is an interesting imaging artifact in the phase image of Figure 3B, which shows a bright crescent at the left of each sphere. Zooming in for a close-up view in Figure 3C,D ($12 \times 12\ \mu m^2$), we see that the larger nanoGUMBOS appear to be less spherically symmetric and occasionally show slight ellipticity. These local views are not fully representative of the range of sizes observed for the entire sample. The corresponding phase image indicates a homogeneous surface composition; a uniformly dark color is observed for nanoGUMBOS regardless of size (Figure 3D). Further, the crescent artifact is not observed in the phase image at this magnification; this and the fact that it only occurs at the left-hand side of the topographical image suggests a tip artifact. Moreover, we note that the size of the AFM tip is quite large compared to the size of the nanoGUMBOS. Likely, the lateral dimensions of the nanoGUMBOS are somewhat broadened by tip−sample convolution.[36,37] The diameters of the nanoGUMBOS were measured based on the reliable *z*-resolution of the AFM acquired from 200 cursor height profiles to confirm the observations from TEM imaging. The heights were referenced to uncovered bare areas of ultraflat mica as a baseline. For all of the areas examined throughout the sample, clusters of aggregated nanoGUMBOS were notably absent. However, due to their spherical shapes, nanoGUMBOS were observed to easily roll across the mica surface, along the direction of scanning, as a result of imaging forces induced during tip motion (data not shown). Therefore, strategies involving low forces and tapping mode are required to prevent unwanted perturbation of the nanoGUMBOS samples during AFM scanning. The images in Figure 3 were acquired using low imaging force, and the nanoparticles were not displaced.

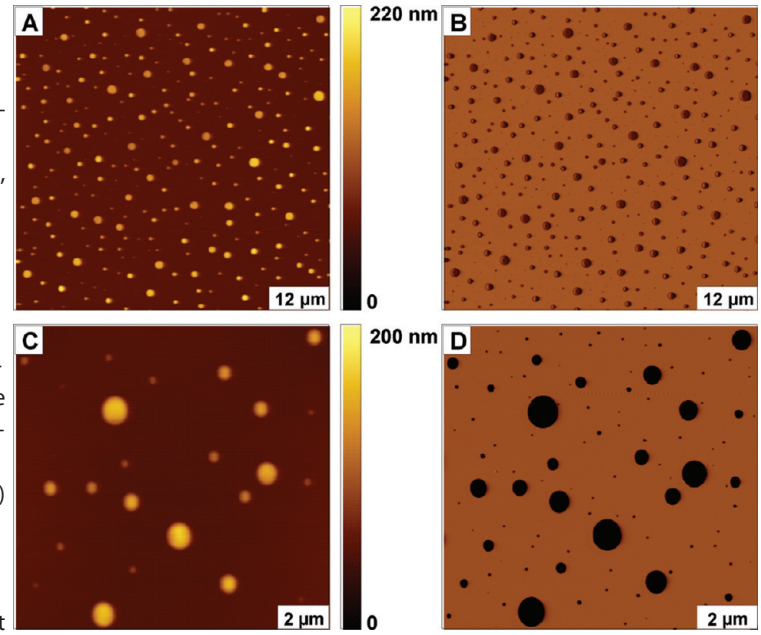

Figure 3. Images of $[Bm_2Im][BF_4]$ nanoGUMBOS synthesized in Scheme 1 acquired with tapping mode AFM at a frequency of 150 kHz. (A) Topographical image ($60 \times 60\ \mu m^2$) and (B) simultaneously acquired phase image. (C) Zoom-in view $12 \times 12\ \mu m^2$ and (D) corresponding phase channel.

Magnetic $[Bm_2Im][FeCl_4]$ GUMBOS Particles. Magnetic $[Bm_2Im][FeCl_4]$ liquid particles (melting point −2.66 °C; see Supporting Information) were similarly produced using the *in situ* ion exchange emulsion method (Scheme 2B). When prepared in bulk, $[Bm_2Im][FeCl_4]$ liquid GUMBOS show three absorption peaks at 528, 617, and 684 nm, which are known to be characteristic of $[FeCl_4^-]$ (see Supporting Information).[27] The liquid particles produced had an average diameter of 98 ± 17 nm when 0.3 M $[Bm_2Im][Cl]$ and 0.3 M $[FeCl_3 \cdot 6H_2O]$ were used for 0.1 M AOT in *n*-heptane ($\omega_0 = 13.34$) based on an optimization study to maximize yield and minimize PDI (data not shown). As the TEM images shown in Figure 4 reveal, a higher number density of spherical magnetic GUMBOS particles was observed when compared with nonmagnetic nanoGUMBOS of similar dimensions. Interestingly, the $[Bm_2Im][FeCl_4]$ particles were densely packed with frequent particle aggregation and overlapping observed in the TEM images. Similar to our results for nonmagnetic nanoGUMBOS discussed above, high reactant concentrations yielded larger particles on average. For the case of increasing the reagent concentration to 0.4 M, all other conditions remaining the same, an effective doubling in particle size to 199 ± 26 nm was obtained (Figure 4B). These larger GUMBOS particles were more spherical and well-segregated on the surface of the

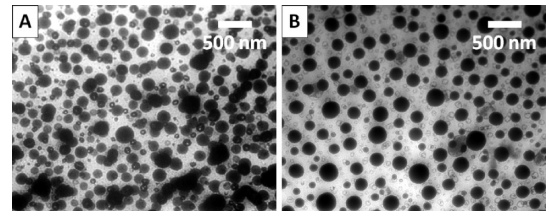

Figure 4. Micrographs of magnetic $[Bm_2Im][FeCl_4]$ GUMBOS particles synthesized in Scheme 1 obtained from TEM revealing mean particle sizes of (A) 98.0 ± 17 nm and (B) 199.0 ± 26 nm. Images were taken using an LVEM5 electron microscope with an accelerating voltage of 5 kV without staining.

TABLE 2. Effect of Reagent Concentration on Particle Size[a]

reagent concentration (M)	particle size (nm)	standard deviation (nm)
0.3	98	17
0.4	199	26

[a] $\omega_0 = 13.34$, molar ratio = 1:1, AOT concentration = 0.1 M.

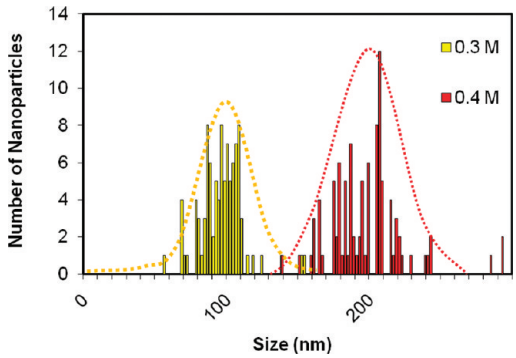

Figure 5. Size distributions of magnetic GUMBOS particles (shown in Figure 4) at various reagent concentrations: [AOT] = 0.1 M; molar reagent concentrations = 0.3 and 0.4 M.

TEM grid. Table 2 clearly shows the increase in diameter of $[Bm_2Im][FeCl_4]$ GUMBOS particles with increasing reagent concentrations. A histogram of the particle size distribution is shown in Figure 5. Surprisingly, in both bases, GUMBOS particles deposited onto freshcleaved mica were well-dispersed and did not form pronounced aggregates. In fact, despite examination of dozens of areas over multiple samples, no clusters or aggregates of $[Bm_2Im][FeCl_4]$ GUMBOS particles were found. This result reflects the role played by surface hydrophobicity during nanoparticle deposition (indeed, there remains little information on how ILs or ionic solids interact with solvate solid surfaces and highlights the soft matter nature of the nanoGUMBOS).[38,39]

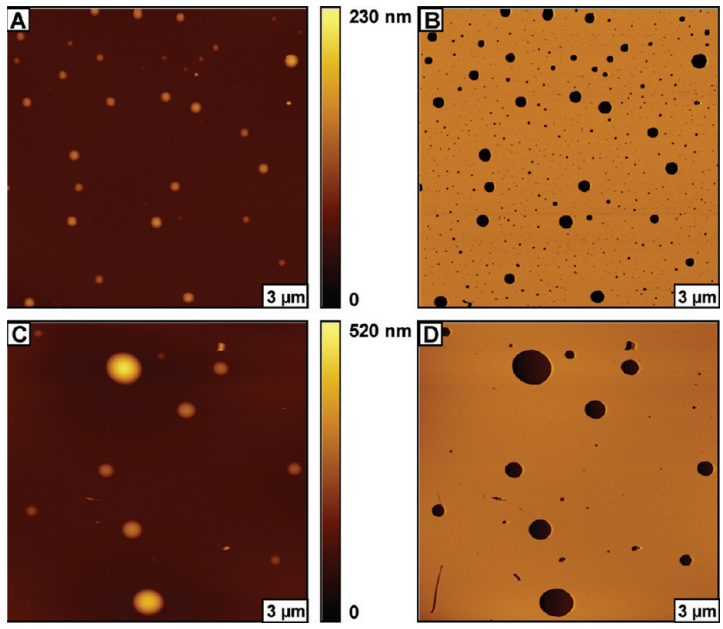

Figure 6. Differently sized samples of magnetic $[Bm_2Im][FeCl_4]$ GUMBOS particles synthesized in Scheme 1 imaged by tapping mode AFM for 20 × 20 μm² scan areas at a 180 kHz driving frequency. (A) Topographical image of magnetic nanoGUMBOS with a diameter near 100 nm and (B) the matching phase image. (C) Topography of 200 nm GUMBOS particles and (D) the corresponding phase frame.

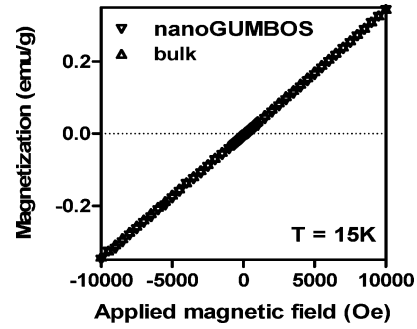

Figure 7. Magnetic susceptibility of bulk $[Bm_2Im][FeCl_4]$ alongside $[Bm_2Im][FeCl_4]$ nanoGUMBOS synthesized in Scheme 1.

Two batches of magnetic GUMBOS particles formed with different target sizes are compared side-by-side in Figure 6. A regular spherical morphology is revealed for 100 nm $[Bm_2Im][FeCl_4]$ nanoGUMBOS (Figure 6A,B). In contrast, in the lower panels of Figure 6, it can be seen that larger magnetic GUMBOS particles sometimes assume slightly egg-shaped morphologies on mica. In both cases, the phase images show uniform dark contrast for the magnetic GUMBOS particles, indicative of a homogeneous surface composition. The phase image of Figure 6B also has the sensitivity to reveal numerous tiny magnetic nanoGUMBOS that were not resolved in the topographical view. Fewer magnetic GUMBOS particles were captured within the 20 × 20 μm² frames of Figures 6C,D for the nominally 200 nm particles. However, the total surface coverage remains nearly the same as that for the 100 nm GUMBOS (approximately 7 and 6% surface coverage is observed in Figure 6B,D, respectively). A few small streak marks were also detected within Figure 6C,D, which is thought to be produced by the action of the AFM tip pushing magnetic GUMBOS particles across the surface. Overall, it is apparent that variations in the amount of reagent in each reverse micelle play a significant role in the sizes of particles produced for both nanoGUMBOS and magnetic GUMBOS particles.

The magnetic properties of bulk magnetic GUMBOS and nanoGUMBOS samples composed of $[Bm_2Im][FeCl_4]$ were investigated using SQUID measurements. In these experiments, bulk $[Bm_2Im][FeCl_4]$ and nanoGUMBOS samples were contained within two separate capsules, and their magnetic moments were measured in the magnetic field range of −10 000 to +10 000 Oe using an MPMS SQUID measuring system. Capsules containing both bulk and nanoscale $[Bm_2Im][FeCl_4]$ GUMBOS show linear responses to the magnetic field, as shown in Figure 7. The magnetic susceptibility of bulk $[Bm_2Im][FeCl_4]$ is 34.3×10^{-6} emu/g

according to the slope of the response to the magnetic field. The magnetic susceptibility of the magnetic nanoGUMBOS sample was identical. In comparison, the magnetic susceptibility of bulk [BmIm][$FeCl_4$] is 40.6 × 10^{-6} emu/g, according to the literature.[27] Similar results were obtained for longer alkyl chain imidazolium-based ILs containing the [$FeCl_4^-$] anion. According to the literature, 1-hexyl-3-methylimidazolium and 1-methy-3-octylimidazolium cations coupled with [$FeCl_4^-$] exhibit magnetic susceptibilities of 39.6 × 10^{-6} and 36.6 × 10^{-6} emu/g, respectively.[40]

CONCLUSION

In summary, a facile and reproducible method for synthesizing controllable sizes of nanoGUMBOS is reported. The ability of nanoGUMBOS to host functional magnetic properties was demonstrated. The overwhelming simplicity and versatility of nanoGUMBOS, particularly illustrated by elaboration of magnetic nanoGUMBOS in the present work, suggest broad application for these emergent nanoscale materials in the biomedical, electronics, analytical, and separations fields.

EXPERIMENTAL SECTION

Materials. 1-Butyl-2,3-dimethylimidazolium chloride [Bm_2Im][Cl] (97%), sodium tetrafluoroborate [Na][BF_4] (99%), iron(III) chloride hexahydrate (Fluka, 98%), sodium bis(2-ethylhexyl)sulfosuccinate (AOT), and *n*-heptane (Sigma, 99%) were purchased from Sigma Aldrich (St. Louis, MO) and used as received. Ultrapure water (18.2 MΩ · cm) was obtained using an Elga model PURELAB ultra water filtration system.

Preparation of NanoGUMBOS and Magnetic GUMBOS Particles. NanoGUMBOS of [Bm_2Im][BF_4] and [Bm_2Im][$FeCl_4$] GUMBOS particles were prepared *via* a modified reverse-micellar method.[35] In a typical preparation, two separate 0.2 M solutions of [Bm_2Im][Cl] and [Na][BF_4] were prepared in ultrapure water. For the magnetic GUMBOS particles preparation, the [$NaBF_4$] was replaced by [$FeCl_3 \cdot 6H_2O$]. Two additional solutions containing 5 mL of 0.1 M AOT in heptane were prepared separately. First, 120 μL of the aqueous [Bm_2Im][Cl] solution was added into 5 mL of 0.1 M AOT solution in heptane, and then 120 μL of the aqueous [Na][BF_4] solution was added into a separate vial also containing 5 mL of 0.1 M AOT solution in heptane. Each solution was then vortexed for 5 min and allowed to equilibrate for 1 h. The molar ratio between [Bm_2Im][Cl] and [Na][BF_4] was 1:1. The two solutions were then mixed in a tightly sealed 20 mL scintillation vial and stirred for 24 h at room temperature. The nanoGUMBOS size can be controlled by varying the concentrations of [Bm_2Im][Cl] and [Na][BF_4]. For 14.7 nm diameter nanoGUMBOS, 0.2 M [Bm_2Im][Cl] and 0.2 M [Na][BF_4] were used. To produce 20.8 nm diameter nanoGUMBOS, 0.4 M [Bm_2Im][Cl] and 0.4 M [Na][BF_4] were used. To synthesize 34.3 nm diameter nanoGUMBOS, 0.5 M [Bm_2Im][Cl] and 0.5 M [Na][BF_4] were used. Last, use of 0.6 M [Bm_2Im][Cl] and 0.6 M [Na][BF_4] afforded 68.0 nm diameter nanoGUMBOS. The magnetic GUMBOS particles sizes could also be controlled by varying the concentrations of [Bm_2Im][Cl] and [$FeCl_3 \cdot 6H_2O$]. For approximately 98 nm diameter nanoGUMBOS, 0.3 M [Bm_2Im][Cl] and 0.3 M [$FeCl_3 \cdot 6H_2O$] were used. Likewise, to produce 199 nm diameter particles, 0.4 M [Bm_2Im][Cl] and 0.4 M [$FeCl_3 \cdot 6H_2O$] were employed, other conditions remaining the same.

UV–Vis Characterization. To characterize the bulk [Bm_2Im][$FeCl_4$], we first measured its visible absorption spectra using a Shimadzu UV-3101PC UV–vis–NIR scanning spectrometer (Shimadzu, Columbia, MD). Absorption was collected using a 1.0 cm^2 quartz cuvette at room temperature, and the blank was subtracted from each spectrum.

Electron Microscopy Characterization. An LVEM5-TEM (Delong America, Montreal, Canada) was used for characterization of the nanoGUMBOS. Samples were prepared by placing 1 μL of the water-in-oil emulsion (w/o) emulsion containing nanoparticles directly onto a carbon-coated copper grid. After 10 min, the grid was immersed in a solution of heptane for 30 s to remove any excess surfactant. The TEM grids were then air-dried at room temperature for 10 min prior to analysis. TEM accelerating voltage was 5 kV. No staining was employed while preparing the TEM samples.

Atomic Force Microscopy Characterization. A Veeco Bioscope scanning probe microscope (SPM) was used for AFM imaging, operated in tapping mode (Veeco Metrology Inc. Santa Barbara, CA). Topography and phase images were acquired with Nanoscope v5.12 software. Digital images were processed with Gwyddion, using Gwyddion open source software, which is freely available on the Internet and supported by the Czech Metrology Institute (http://gwyddion.net/). Silicon cantilevers with resonance frequency range of 146–236 kHz and spring constants ranging from 21 to 98 N/m were used to acquire tapping mode images (Nanosensor, Lady's Island, SC). Estimates of surface coverage were obtained with UTHSCA Image Tool for Windows version 3.00 (San Antonio, TX). The percentage of colored pixels was determined subjectively to provide estimates of surface coverage. The topography images were converted to grayscale bitmaps, and a threshold value was selected visually for conversion to black and white pixels for quantitative comparisons. Solutions of nanoGUMBOS and magnetic nanoGUMBOS were diluted in heptane and deposited on freshly cleaved pieces (1 × 1 cm^2) of Ruby muscovite mica (S&J Trading Co., NY). Samples were dried for at least 48 h then imaged in ambient air using tapping mode AFM.

Acknowledgment. I.M.W. acknowledges the National Science Foundation, the National Institutes of Health, and the Philip W. West Endowment for support of this work. The authors thank Dr. John F. DiTusa for assistance in the SQUID measurements, and Sergio de Rooy for technical assistance.

Supporting Information Available: UV–vis absorption spectrum of [Bm_2Im][$FeCl_4$] and determination of [Bm_2Im][$FeCl_4$] melting point using DSC. This material is available free of charge *via* the Internet at http://pubs.acs.org.

REFERENCES AND NOTES

1. Baker, G. A.; Baker, S. N.; Pandey, S.; Bright, F. V. An Analytical View of Ionic Liquids. *Analyst* **2005**, *130*, 800–808.
2. Rogers Robin, D.; Seddon Kenneth, R. Chemistry. Ionic Liquids—Solvents of the Future. *Science* **2003**, *302*, 792–793.
3. Del Popolo, M. G.; Voth, G. A. On the Structure and Dynamics of Ionic Liquids. *J. Phys. Chem. B* **2004**, *108*, 1744–1752.
4. Tran, C. D.; Oliveira, D. Fluorescence Determination of Enantiomeric Composition of Pharmaceuticals *via* Use of Ionic Liquid That Serves as Both Solvent and Chiral Selector. *Anal. Biochem.* **2006**, *356*, 51–58.
5. Huddleston, J. G.; Rogers, R. D. Room Temperature Ionic Liquids as Novel Media for 'Clean' Liquid–Liquid Extraction. *Chem. Commun.* **1998**, 1765–1766.
6. Ding, J.; Welton, T.; Armstrong, D. W. Chiral Ionic Liquids as Stationary Phases in Gas Chromatography. *Anal. Chem.* **2004**, *76*, 6819–6822.
7. Visser, A. E.; Swatloski, R. P.; Reichert, W. M.; Mayton, R.; Sheff, S.; Wierzbicki, A.; Davis, J. H., Jr.; Rogers, R. D. Task-Specific Ionic Liquids Incorporating Novel Cations for the Coordination and Extraction of Hg^{2+} and Cd^{2+}: Synthesis,

Characterization, and Extraction Studies. *Environ. Sci. Technol.* **2002**, *36*, 2523–2529.
8. Earle, M. J.; Seddon, K. R.; Adams, C. J.; Roberts, G. Friedel–Crafts Reactions in Room Temperature Ionic Liquids. *Chem. Commun.* **1998**, 2097–2098.
9. Zheng, W.; Liu, X.; Yan, Z.; Zhu, L. Ionic Liquid-Assisted Synthesis of Large-Scale TiO_2 Nanoparticles with Controllable Phase by Hydrolysis of $TiCl_4$. *ACS Nano* **2009**, *3*, 115–122.
10. Kuang, D.; Brillet, J.; Chen, P.; Takata, M.; Uchida, S.; Miura, H.; Sumioka, K.; Zakeeruddin, S. M.; Gratzel, M. Application of Highly Ordered TiO_2 Nanotube Arrays in Flexible Dye-Sensitized Solar Cells. *ACS Nano* **2008**, *2*, 1113–1116.
11. Gao, S.; Zhang, H.; Wang, X.; Mai, W.; Peng, C.; Ge, L. Palladium Nanowires Stabilized by Thiol-Functionalized Ionic Liquid: Seed-Mediated Synthesis and Heterogeneous Catalyst for Sonogashira Coupling Reaction. *Nanotechnology* **2005**, *16*, 1234–1237.
12. Ryu, H. J.; Sanchez, L.; Keul, H. A.; Raj, A.; Bockstaller, M. R. Imidazolium-Based Ionic Liquids as Efficient Shape-Regulating Solvents for the Synthesis of Gold Nanorods. *Angew. Chem., Int. Ed.* **2008**, *47*, 7639–7643.
13. Zhou, S.; Ma, Z.; Baker, G. A.; Rondinone, A. J.; Zhu, Q.; Luo, H.; Wu, Z.; Dai, S. Self-Assembly of Metal Oxide Nanoparticles into Hierarchically Patterned Porous Architectures Using Ionic Liquid/Oil Emulsions. *Langmuir* **2009**, *25*, 7229–7233.
14. Rutten, F. J. M.; Tadesse, H.; Licence, P. Rewritable Imaging on the Surface of Frozen Ionic Liquids. *Angew. Chem., Int. Ed.* **2007**, *46*, 4163–4165.
15. Tesfai, A.; El-Zahab, B.; Bwambok, D. K.; Baker, G. A.; Fakayode, S. O.; Lowry, M.; Warner, I. M. Controllable Formation of Ionic Liquid Micro- and Nanoparticles *via* a Melt–Emulsion–Quench Approach. *Nano Lett.* **2008**, *8*, 897–901.
16. Giri, S.; Trewyn, B. G.; Stellmaker, M. P.; Lin, V. S. Y. Stimuli-Responsive Controlled-Release Delivery System Based on Mesoporous Silica Nanorods Capped with Magnetic Nanoparticles. *Angew. Chem., Int. Ed.* **2005**, *44*, 5038–5044.
17. Nunez, L.; Kaminski, M. D. Transuranic Separation Using Organophosphorus Extractants Adsorbed onto Superparamagnetic Carriers. *J. Magn. Magn. Mater.* **1999**, *194*, 102–107.
18. Mornet, S.; Vasseur, S.; Grasset, F.; Veverka, P.; Goglio, G.; Demourgues, A.; Portier, J.; Pollert, E.; Duguet, E. Magnetic Nanoparticle Design for Medical Applications. *Prog. Solid State Chem.* **2006**, *34*, 237–247.
19. Gupta, A. K.; Gupta, M. Synthesis and Surface Engineering of Iron Oxide Nanoparticles for Biomedical Applications. *Biomaterials* **2005**, *26*, 3995–4021.
20. Lu, A. H.; Salabas, E. L.; Schueth, F. Magnetic Nanoparticles: Synthesis, Protection, Functionalization, and Application. *Angew. Chem., Int. Ed.* **2007**, *46*, 1222–1244.
21. Hong, X.; Li, J.; Wang, M.; Xu, J.; Guo, W.; Li, J.; Bai, Y.; Li, T. Fabrication of Magnetic Luminescent Nanocomposites by a Layer-by-Layer Self-assembly Approach. *Chem. Mater.* **2004**, *16*, 4022–4027.
22. Jeong, J.-R.; Lee, S.-J.; Kim, J.-D.; Shin, S.-C. Magnetic Properties of Fe_3O_4 Nanoparticles Encapsulated with Poly(D,L-lactide-*co*-glycolide). *IEEE Trans. Magn.* **2004**, *40*, 3015–3017.
23. Ohno, H.; Fukumoto, K. Amino Acid Ionic Liquids. *Acc. Chem. Res.* **2007**, *40*, 1122–1129.
24. Hough-Troutman, W. L.; Smiglak, M.; Griffin, S.; Reichert, W. M.; Mirska, I.; Jodynis-Liebert, J.; Adamska, T.; Nawrot, J.; Stasiewicz, M.; Rogers, R. D.; Pernak, J. Ionic Liquids with Dual Biological Function: Sweet and Anti-Microbial, Hydrophobic Quaternary Ammonium-Based Salts. *New J. Chem.* **2009**, *33*, 26–33.
25. Hough, W. L.; Smiglak, M.; Rodriguez, H.; Swatloski, R. P.; Spear, S. K.; Daly, D. T.; Pernak, J.; Grisel, J. E.; Carliss, R. D.; Soutullo, M. D.; Davis, J. J. H.; Rogers, R. D. The Third Evolution of Ionic Liquids: Active Pharmaceutical Ingredients. *New J. Chem.* **2007**, *31*, 1429–1436.
26. Del Sesto, R. E.; McCleskey, T. M.; Burrell, A. K.; Baker, G. A.; Thompson, J. D.; Scott, B. L.; Wilkes, J. S.; Williams, P. Structure and Magnetic Behavior of Transition Metal Based Ionic Liquids. *Chem. Commun.* **2008**, 447–449.
27. Hayashi, S.; Hamaguchi, H.-O. Discovery of a Magnetic Ionic Liquid [Bmim]$FeCl_4$. *Chem. Lett.* **2004**, *33*, 1590–1591.
28. Hayashi, S.; Saha, S.; Hamaguchi, H.-O. A New Class of Magnetic Fluids: Bmim[$FeCl_4$] and Nbmim[$FeCl_4$] Ionic Liquids. *IEEE Trans. Magn.* **2006**, *42*, 12–14.
29. Freire, M. G.; Neves, C. M. S. S.; Carvalho, P. J.; Gardas, R. L.; Fernandes, A. M.; Marrucho, I. M.; Santos, L. M. N. B. F.; Coutinho, J. A. P. Mutual Solubilities of Water and Hydrophobic Ionic Liquids. *J. Phys. Chem. B* **2007**, *111*, 13082–13089.
30. Choudhury, A. R.; Winterton, N.; Steiner, A.; Cooper, A. I.; Johnson, K. A. *In Situ* Crystallization of Low-Melting Ionic Liquids. *J. Am. Chem. Soc.* **2005**, *127*, 16792–16793.
31. Motte, L.; Billoudet, F.; Pileni, M. P. Self-Assembled Monolayer of Nanosized Particles Differing by Their Sizes. *J. Phys. Chem.* **1995**, *99*, 16425–16429.
32. Wu, M.-L.; Chen, D.-H.; Huang, T.-C. Synthesis of Au/Pd Bimetallic Nanoparticles in Reverse Micelles. *Langmuir* **2001**, *17*, 3877–3883.
33. Uskokovic, V.; Drofenik, M. Synthesis of Materials within Reverse Micelles. *Surf. Rev. Lett.* **2005**, *12*, 239–277.
34. Eastoe, J.; Gold, S.; Rogers, S. E.; Paul, A.; Welton, T.; Heenan, R. K.; Grillo, I. Ionic Liquid-in-Oil Microemulsions. *J. Am. Chem. Soc.* **2005**, *127*, 7302–7303.
35. Harruff, B. A.; Bunker, C. E. Spectral Properties of AOT-Protected CdS Nanoparticles: Quantum Yield Enhancement by Photolysis. *Langmuir* **2003**, *19*, 893–897.
36. Schwarz, U. D.; Haefke, H.; Reimann, P.; Guentherodt, H. J. Tip Artifacts in Scanning Force Microscopy. *J. Microsc.* **1994**, *173*, 183–197.
37. Ramirez-Aguilar, K. A.; Rowlen, K. L. Tip Characterization from AFM Images of Nanometric Spherical Particles. *Langmuir* **1998**, *14*, 2562–2566.
38. Gao, L.; McCarthy, T. J. Ionic Liquids Are Useful Contact Angle Probe Fluids. *J. Am. Chem. Soc.* **2007**, *129*, 3804–3805.
39. Kilaru, P.; Baker, G. A.; Scovazzo, P. Density and Surface Tension Measurements of Imidazolium-, Quaternary Phosphonium-, and Ammonium-Based Room-Temperature Ionic Liquids: Data and Correlations. *J. Chem. Eng. Data* **2007**, *52*, 2306–2314.
40. Yoshida, Y.; Saito, G. Influence of Structural Variations in 1-Alkyl-3-methylimidazolium Cation and Tetrahalogenoferrate(III) Anion on the Physical Properties of the Paramagnetic Ionic Liquids. *J. Mater. Chem.* **2006**, *16*, 1254–1262.